


 CrossMark  
 click for updates

 Cite this: *Soft Matter*, 2014, 10, 8157

 Received 17th June 2014  
 Accepted 29th August 2014

DOI: 10.1039/c4sm01299b

[www.rsc.org/softmatter](http://www.rsc.org/softmatter)

## Hybrid hydrogel sheets that undergo pre-programmed shape transformations†

 Zengjiang Wei,<sup>ab</sup> Zheng Jia,<sup>c</sup> Jasmin Athas,<sup>d</sup> Chaoyang Wang,<sup>b</sup> Srinivasa R. Raghavan,<sup>d</sup> Teng Li<sup>\*c</sup> and Zhihong Nie<sup>\*a</sup>

This communication describes a novel strategy to achieve programmable shape transformation of hybrid hydrogel sheets by modulating both the in-plane and out-of-plane mismatches in mechanical properties. Both our experimental and computational results demonstrate that the shape transformation of hybrid hydrogel sheets shows rich features (e.g., rolling direction, axis, chirality, etc.) and versatile tunability (e.g., via various external stimuli, material properties, pattern geometry, etc.). This work can provide guidance for designing soft materials that are able to undergo more precise and complex shape transformation.

Shape-transforming phenomena are ubiquitous in living things such as plants. For example, the Venus flytrap can open and close the terminal portion of its leaves, and awns of wild oats rearrange into helices upon desiccation. Such phenomena have inspired the synthesis and design of artificial “smart” systems that can sense changes and adjust their shapes in response to the environment, much as in living organisms.<sup>1–6</sup> The tremendous interest in self-shaping materials stems from their wide range of potential applications, ranging from biomedical devices to optoelectronics. Particularly, shape-transforming hydrogels are attractive because of their tunable responsiveness to stimuli such as temperature, humidity, ionic strength variation, pH, electric current, and light.<sup>7–20</sup> These materials have numerous potential applications in soft robotics,<sup>12</sup> as self-

healing materials,<sup>21,22</sup> in drug delivery,<sup>23</sup> as reactors,<sup>24</sup> actuators,<sup>25</sup> and in three-dimensional (3D) cell culture.<sup>26</sup>

The modulation of sheet-like soft materials (e.g., hydrogels) to induce simple bending and twisting has been widely explored since the early report by Hu *et al.*<sup>27</sup> Bending of gel sheets primarily relies on the inhomogeneity in the volumetric variation (namely, swelling or shrinking) along the sheet thickness direction in response to stimuli. This is frequently achieved by utilizing bilayer or gradient structures along the thickness direction. Programming soft materials to attain complex 3D shape transformations was not explored until recently. Commonly used strategies usually involve the multi-step folding of isotropic, stimuli-responsive polymer bilayers to fabricate complex 3D structures like pyramidal cones, multi-arm stars and tubular constructs.<sup>5,8,16,19,28–32</sup> These methods are based on a hinge-like mechanism and are not capable of creating complex structures with well-defined curvatures.<sup>28</sup> Recently, the modulation of local in-plane stress (without differential volume change along thickness) within sheets has been proven to be a powerful methodology of programming the formation of highly complex shapes.<sup>17,33–35</sup> These structures are not attainable by conventional approaches based on bilayer or gradient structures. However, relatively small differentiation in in-plane stresses results in limited driving forces to induce shape transformation at large amplitudes. Our hypothesis is that the combination of two strategies, *i.e.*, internal stress modulation and bilayer structure (Fig. 1a), would be sufficient to create unique shape-transforming hydrogels that would be otherwise impossible to create using each strategy individually. In this case, the bilayer morphology of the hydrogel provides a sufficiently large driving force to transform as-made 2D hydrogel sheets into 3D, while the compositional patterns enable small-scale modulation of internal stress, which in turn renders programmable tunability of the shape transformation.

Without an external mechanical load or geometric constraints, a homogeneous hydrogel network equilibrates with the surrounding solvent by a homogenous and isotropic deformation. Such free swelling can be analytically studied

<sup>a</sup>Department of Chemistry and Biochemistry, University of Maryland, College Park, MD 20742, USA. E-mail: [znie@umd.edu](mailto:znie@umd.edu)

<sup>b</sup>Research Institute of Materials Science, South China University of Technology, Guangzhou 510640, China

<sup>c</sup>Department of Mechanical Engineering, University of Maryland, College Park, MD 20742, USA. E-mail: [LiT@umd.edu](mailto:LiT@umd.edu)

<sup>d</sup>Department of Chemical and Biomolecular Engineering, University of Maryland, College Park, MD 20742-2111, USA

† Electronic supplementary information (ESI) available: The synthesis recipe and experimental details, simulation process, and shape transformation of this hybrid hydrogel response to temperature and ion concentration. See DOI: 10.1039/c4sm01299b

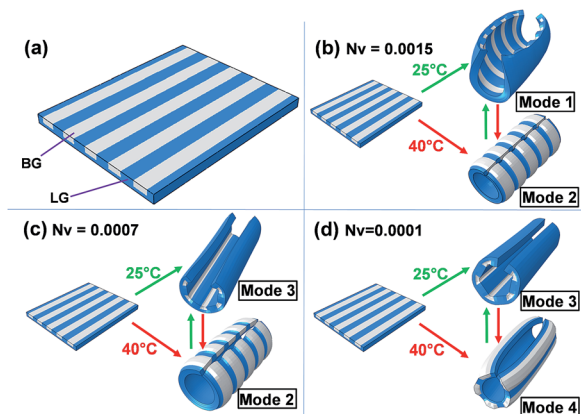


Fig. 1 Shape transformations predicted by FEM. (a) Schematic of an as-made bilayer hybrid hydrogel sheet. The blue colour represents the laponite-crosslinked gels (LGs), while the white colour indicates the  $N,N'$ -methylene-bis-acrylamide (BIS)-crosslinked gels (BGs). (b–d) Modelling of shape transformation of hybrid hydrogel sheets with a normalized nominal density of polymer chains of BG of  $Nv = 0.0015$  (b),  $0.0007$  (c) and  $0.0001$  (d). Here  $N$  is the nominal density of polymer chains of BG and  $v$  is the volume of one water molecule. The resulting shape of hybrid hydrogel sheets submerged in  $25\text{ }^{\circ}\text{C}$  or  $40\text{ }^{\circ}\text{C}$  water can be categorized into four modes (denoted as Modes 1, 2, 3 and 4), based on the rolling direction and orientation of the rolling axis.

using a thermodynamic framework. However, free swelling of hydrogels rarely occurs in nature. In real scenarios, an anisotropic or an inhomogeneous state of deformation occurs in response to an external mechanical load or geometric constraint. To elucidate such inhomogeneous deformation, finite element modeling (FEM) has been implemented recently to study hydrogel deformation under various stimuli and constraints.<sup>36</sup>

Herein, we report the FEM-assisted design of 2D hydrogel sheets with programmable capability to undergo specific shape transformations. The hybrid hydrogel sheets fabricated by multi-step photolithography comprise laponite-crosslinked gels (LGs) and  $N,N'$ -methylene-bis-acrylamide (BIS)-crosslinked gels (BGs) (see details of fabrication in the ESI†).<sup>37</sup> The LGs are made from poly( $N$ -isopropyl acrylamide) (PNIPAm) cross-linked using nanoparticles of a synthetic clay called laponite.<sup>38</sup> The cross-linking of PNIPAm by laponite proceeds by a free-radical polymerization, while the bonds between laponite and PNIPAm chains are suggested to be non-covalent (polar or ionic).<sup>39–43</sup> The BGs are PNIPAm gels covalently cross-linked by a conventional multifunctional crosslinker, BIS (see detailed recipes in the ESI†). The PNIPAm gel shows a Lower Critical Solution Temperature (LCST) of  $\sim 32\text{ }^{\circ}\text{C}$ , above which it dehydrates and shrinks. The LGs and BGs show significant difference in elastic modulus and volumetric change in response to external stimuli (e.g., temperature, salt, or solvent).<sup>44,45</sup> The LGs are softer and swell/shrink more than the BGs. The planar hydrogel sheets comprise two layers: the top layer consists of alternating slender strips of LGs and BGs, and the bottom layer is pure LG (Fig. 1a). These hybrid hydrogel sheets undergo a unique shape transformation that is beyond the capability of conventional

strategies. We demonstrate that the hybrid hydrogel sheets transform between left-handed and right-handed helices, between tubes with the top or the bottom sheet surface selectively hidden inside, or between tubular states with different rolling axes in both experiments and simulations. Our study provides a mechanistic understanding on the parameters that govern these shape transformations. We are thus able to offer guidelines to further explore the opportunities afforded by our design strategy.

We started with continuum modeling to investigate the shape transformation of the hybrid hydrogel sheets (Fig. 1b–d). In all simulations, the BG strips are perpendicular to the long axis of the hydrogel sheet (Fig. 1a). The material properties of the BG and LG are characterized by the nominal density of polymer chains and the enthalpy of mixing. Here, the nominal density of polymer chains describes the number of polymer chains divided by the volume of dry polymer, and the enthalpy of mixing is a measure of the strength of pairwise interactions between polymers and the solvent (see details in the ESI†). Our simulations suggest that these two parameters play a critical role in the shape transformation of the hybrid hydrogel sheets. Variation in nominal density of polymer chains or enthalpy of mixing may significantly affect the response (e.g. volume change, etc.) of LG and BG to external stimuli, thus resulting in different morphologies of hybrid hydrogel sheets (Fig. 1b–d).

To demonstrate different possible morphologies, we studied hybrid hydrogel sheets with three representative nominal densities of polymer chains in the BG while all other material properties of BGs and LGs are taken to be the same in these three cases (listed in Table S1†). Fig. 1b illustrates shape transformation of hybrid hydrogel sheets with  $Nv = 0.0015$ , where  $N$  is the nominal density of polymer chains of BG and  $v$  represents the volume of one water molecule.  $Nv$  is normalized nominal density of polymer chains and is defined as a dimensionless measurement of the polymer chain density. Submerged in pure water at  $25\text{ }^{\circ}\text{C}$ , LG absorbs more water and hence swells more than BG does, resulting in the rolling up of the 2D hydrogel sheet into a tubular structure with the BG strips hidden inside the tube (denoted as Mode 1). When the water temperature is switched to  $40\text{ }^{\circ}\text{C}$ , beyond the LCST of the constituent PNIPAm gels, both LG and BG dehydrate and shrink in volume, with the LG shrinking more than the BG. As a result, the tubular hybrid hydrogel sheet in Mode 1 first opens up and flattens, then further rolls into a tubular structure with the BG strips exposed outside (denoted as Mode 2). Moreover, the shape transition between Mode 1 and Mode 2 is fully reversible and repeatable. The rolling direction (so that BG strips are exposed outside or hidden inside) is mainly determined by the difference between the volumetric swelling of BG and LG,  $\Delta v = \Delta v_{\text{BG}} - \Delta v_{\text{LG}}$ , where  $\Delta v_{\text{BG}}$  and  $\Delta v_{\text{LG}}$  can, in principle, be fully specified by the material properties of PNIPAm gels and the solvent environment. Negative  $\Delta v$  results in morphologies with the BG strips hidden inside, while positive  $\Delta v$  renders morphologies with the BG strips exposed outside. Besides the rolling direction, the final shape of a hybrid hydrogel sheet is also characterized by the rolling axis, which is perpendicular to the BG strips in both Mode 1 and Mode 2.

Shape transformation of hybrid hydrogel sheets with  $N\nu = 0.0007$  of BG is shown in Fig. 1c. While submerging the sheet into 40 °C water results in a tubular structure with BG strips exposed outside and a rolling axis perpendicular to BG strips (*i.e.*, Mode 2 as in Fig. 1b), decreasing water temperature to 25 °C first leads to the flattening of the tubular structure in Mode 2, followed by further rolling about an axis parallel to the BG strips into another tubular structure with BG strips hidden inside (denoted as Mode 3). The transition between Mode 2 and Mode 3 is also fully reversible and repeatable. When the normalized nominal density of polymer chains of BG is taken to be 0.0001 (Fig. 1d), the hybrid hydrogel sheet rolls up along an axis parallel to the BG strips into a tubular structure with BG strips hidden inside when submerged in 25 °C water (*i.e.*, Mode 3 as in Fig. 1c), but with BG strips exposed outside when submerged in 40 °C water (denoted as Mode 4). The transition between Mode 3 and Mode 4 here is also fully reversible and repeatable. Characteristics of the abovementioned four modes of 3D shape transformation from the as-made 2D hybrid hydrogel sheets are summarized in Table S2.† The modeling study shown in Fig. 1 indicates that the change of nominal density of polymer chains of BG can lead to the switching of the rolling axis of the hybrid hydrogel sheets. In addition, the enthalpy of mixing and geometry of BG/LG strips may also have influence on the rolling axis, which requires further systematic numerical studies beyond the scope of this paper and will be presented elsewhere.

Instructed by the findings from simulations, we have explored the shape transformation of hybrid hydrogel sheets with designed LG/BG strips. The sheets were fabricated as described in the ESI.† The shape transformation was triggered by placing the sheet in water at controlled temperatures. We started with hybrid hydrogels with low crosslinking density of BGs ( $C_{\text{BIS}} < 5$  mol%). In this case, the stiffness of BGs is comparable to that of LGs. The as-fabricated sheets remained flat on the substrate at room temperature (25 °C). When the sheets were immersed in water at 25 °C, the LG portions expand more than the BG portions. To accommodate the volume mismatch, the hybrid BG/LG sheets bent towards the BG-strip (top) side about an axis perpendicular to the BG strips, thus leading to the formation of a tubular structure with the BG strips hidden in the interior of the tube (left panel in Fig. 2a), as predicted by Mode 1 in the simulations (Fig. 1b). When the resulting tubular structure was moved to water having an elevated temperature of 40 °C, both the LG and BG portions shrank and expelled water, with the LGs shrinking more than the BGs. During this process, the tubes first opened up and became flat, and then continuously bent towards the all-LG sides, leading to another tubular structure with the BG strips exposed outside (right panel in Fig. 2a), as predicted by Mode 2 in the simulations (Fig. 1b). We thus see a good agreement between the simulation results and the experimental observations, including in the fine features such as the overall fusiform shape with BG strips wrapped inside in Mode 1 (Fig. 2b) and the surface undulation morphology with BGs at peaks and LGs at troughs in Mode 2 (Fig. 2c). It is worth noting that the formation of the fusiform shape in Mode 1 results from the bending of

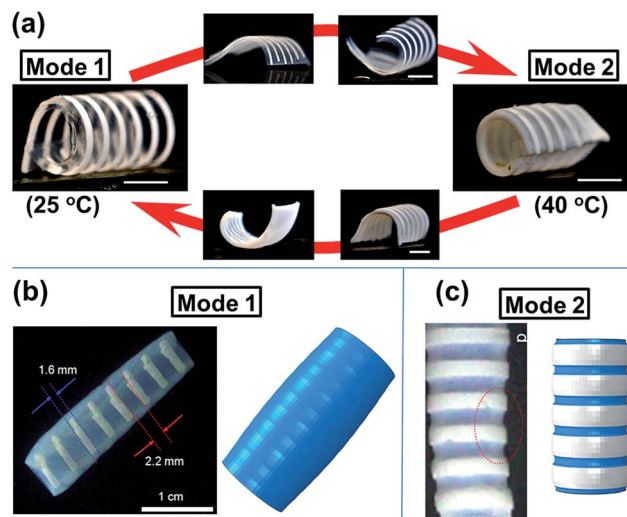


Fig. 2 Experimental demonstration of the shape transformation of hybrid hydrogel sheets. (a) Reversible and repeatable transition between Modes 1 and 2, as predicted by simulations. Excellent agreement is seen between the shapes predicted by simulation and those observed experimentally, including fine details such as: (b) overall fusiform shape in Mode 1; (c) surface undulation morphology in Mode 2. The scale bar is 1 cm.

sheets along two competing axes as aforementioned: the axis parallel to and that perpendicular to the BG strips. In Mode 1, the bending along the rolling axis normal to the BG strips dominates the deformation of the hybrid hydrogel sheet; but the sheet also tends to roll up along the axis parallel to the BG strips, especially at its four free corners (Fig. 1b). This combined deformation led to the overall fusiform shape, which proves the existence of the two rolling axes predicted by simulations. Further placement of the tubular hydrogel sheet in Mode 2 into water at 25 °C made the sheets recover its original tubular structure in Mode 1 (see both Experimental and computational time-dependent transformation in the ESI†). This indicates that the entire shape-transformation is reversible and repeatable. Shape transformations of the hybrid hydrogel sheets can also be achieved by tuning the ionic strength of water or the composition of solvents (*e.g.*, the addition of ethanol, see details in the ESI†). Both simulations and experiments suggest that the differential volume change in a hydrogel bilayer induces strong and localized internal stresses and determines the rolling direction of the hydrogel sheets, while the asymmetric spatial arrangement of the gel strips serves as the geometric origin of its preferential rolling axis.

To quantitatively understand the shape transformation mechanism, we examined the variation in the width of the BG ( $W_{\text{BG}}$ ) and LG ( $W_{\text{LG}}$ ) strips during shape transformation as a function of time after a tubular hydrogel sheet in Mode 1 was first immersed in 40 °C water and then in 25 °C water (Fig. 3 and S6†). In 40 °C water, both LG and BG shrank, but  $W_{\text{LG}}$  decreased faster than  $W_{\text{BG}}$ , as indicated by the steeper slope of the black curve in Fig. 3a. Meanwhile, the tubular sheet first unfolded and became flat, and then bent further in the opposite direction to form another tubular structure in Mode 2 (Fig. 3b) in ~40 min.

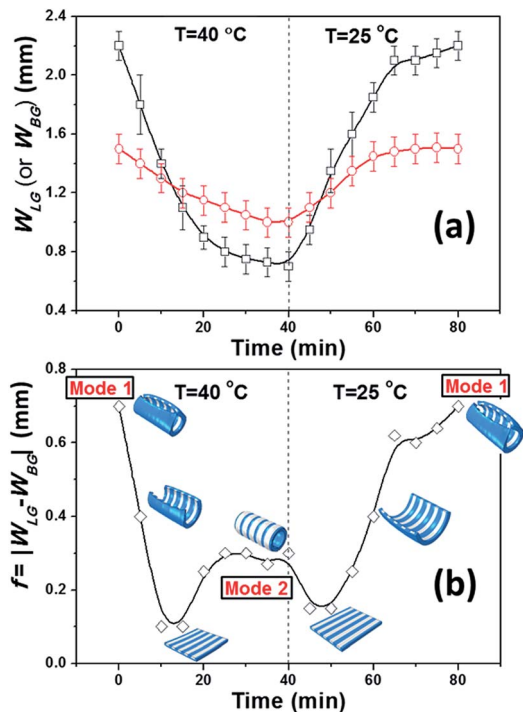


Fig. 3 (a) Variation in the BG strip width  $W_{BG}$  (red) and LG strip width  $W_{LG}$  (dark), and (b) the difference between  $W_{LG}$  and  $W_{BG}$  of the hybrid hydrogel sheet, as a function of time after a tubular hydrogel sheet in Mode 1 is first immersed in 40 °C water and then in 25 °C water. The data points are obtained by measuring the dimensions of hydrogel sheets. Computational images in (b) show the reversible transition from Mode 1 to Mode 2 and back to Mode 1.

When this Mode 2 tubular structure was then immersed in 25 °C water, both BG and LG swelled, but  $W_{LG}$  increased faster than  $W_{BG}$ . While swelling, the Mode 2 tubular structure flattened first and then bent further to recover into a tubular structure in Mode 1 in ~40 min. This clearly demonstrates the reversible transition between different shapes. The plot of  $f = W_{LG} - W_{BG}$  as a function of time (Fig. 3b) reveals that tubular structures were formed at peak values of  $f$ , while the sheet was flat when  $f$  is at its minima.

The simulations demonstrate that the normalized nominal density of polymer chains in BGs strongly affects the shape transformation of the hybrid hydrogel sheets. It is noted that the nominal density of polymer chains  $N$  depends on the crosslink density of the hydrogels. Inspired by these simulation findings, we then varied the crosslink densities of the constituent hydrogels and studied the resultant effects on the shape transformation of the hybrid hydrogel sheets. For this, we varied the elastic modulus (under shear) of the BGs ( $G_{BG}$ ) by varying the concentration of the crosslinker (BIS) and hence the crosslinking density of the gels. At the same time, we maintained the elastic modulus of the LGs ( $G_{LG}$ ) at ~425 Pa. Fig. 4 shows that as the concentration of BIS,  $C_{BIS}$ , increased from 3 to 7 mol% and  $G_{BG}$  increased from ~1000 to ~20 000 Pa. When hybrid hydrogel sheets with various BG/LG stiffness ratios were immersed in 25 °C water, we found that there is a threshold value of  $C_{BIS}$  (5 mol%), below which the sheets rolled along an

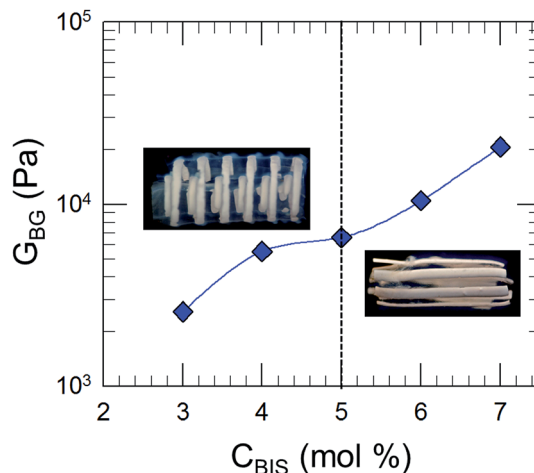


Fig. 4 The elastic modulus in shear of the BG,  $G_{BG}$  as a function of the concentration of the BIS crosslinker. The elastic modulus of the LG is constant ( $G_{LG} \sim 425$  Pa). Corresponding BG/LG hybrid gels attain shapes depending on the relative values of  $G_{BG}$  and  $G_{LG}$ , as shown by the photographs in the insets.

axis perpendicular to the BG strips (Mode 1) while above which the sheets rolled along an axis parallel to the BG strips (Mode 3). The competition between two rolling axes can be explained by the following energetics: the free energy of the hydrogels is composed of the energy due to the stretching of the polymeric network (*i.e.*, the elastic energy) and the energy due to the mixing of the gel with the solvent. The elastic energy of the hydrogel sheets scales with the stiffness of the BG and LG strips. As  $C_{BIS}$  increases, the BG strips become stiffer. Above a threshold value of BG stiffness, rolling along an axis perpendicular to the BG strips becomes energetically unfavorable, thus gives way to rolling along an axis parallel to the BG strips which results in minimal deformation of the stiffer BG strips. Nonetheless, comprehensive understanding of the competition between rolling axes and its quantitative dependence on the material properties of the BG and LG still requires further systematic investigation.

Finally, we demonstrate the reversible switching of hydrogel sheets between states of different chiralities. To obtain helical shapes, the hybrid hydrogel sheet was cut along a slant so that the slender strips made an angle of  $\sim 45^\circ$  with respect to the long axis of the sheet (see Fig. S3<sup>†</sup>). The immersion of such a hydrogel sheet in 25 °C water led to a right-handed helical structure, by bending along the direction parallel to the BG strips (Fig. 5a). When the right-handed helix was placed in 40 °C water, the helix flattened and then further rolled into a similar helical structure but with opposite chirality, *i.e.*, a left-handed helix (Fig. 5b). This transformation was also repeatable and reversible. Such a transition may find potential applications in programming the optical and electronic properties of soft materials and devices.

In summary, we have developed a novel strategy to achieve programmable shape transformation of hybrid hydrogel sheets by modulating both the in-plane and out-of-plane mismatches in mechanical properties. Both our experimental and

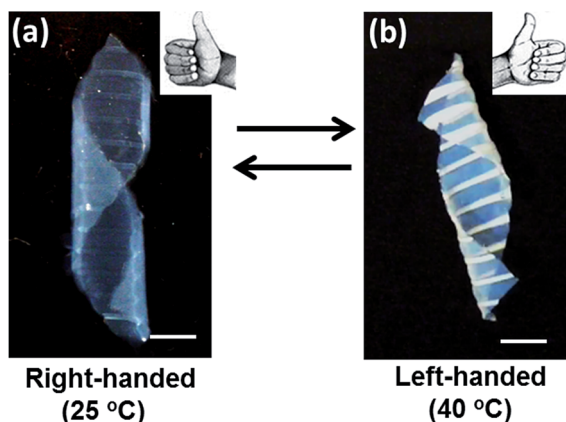


Fig. 5 Experimental demonstration of the reversible switching of a hybrid hydrogel sheet from a right-handed helix at 25 °C to a left-handed helix at 40 °C. Here, the slender strips of BG are at an angle of 45° relative to the long axis of the LG sheet. The scale bar is 1 cm.

computational results demonstrate rich features (*e.g.*, rolling direction, axis, chirality, *etc.*) and versatile tunability (*e.g.*, *via* various external stimuli, material properties, pattern geometry, *etc.*). The general principle emerging from the present study can be applied to design soft materials that are able to undergo more precise and complex shape transformation and thus may find potential applications in drug delivery, actuators, sensors, tissue engineering, and optical and electronic devices.

## Conflict of interest

The authors declare no competing financial interests.

## Acknowledgements

ZN acknowledges the financial support from the University of Maryland. TL and ZJ are grateful for the support of NASA (Grant number: NNX12AM02G). ZJ acknowledges a UMD Graduate Dean's Dissertation Fellowship. ZW thanks the support of China Scholarship Council.

## References

- X. M. He, M. Aizenberg, O. Kuksenok, L. D. Zarzar, A. Shastri, A. C. Balazs and J. Aizenberg, *Nature*, 2012, **487**, 214–218.
- A. W. Feinberg, A. Feigel, S. S. Shevkoplyas, S. Sheehy, G. M. Whitesides and K. K. Parker, *Science*, 2007, **317**, 1366–1370.
- J. R. Capadona, K. Shanmuganathan, D. J. Tyler, S. J. Rowan and C. Weder, *Science*, 2008, **319**, 1370–1374.
- P. Fratzl, *J. R. Soc., Interface*, 2007, **4**, 637–642.
- M. Jamal, N. Bassik, J. H. Cho, C. L. Randall and D. H. Gracias, *Biomaterials*, 2010, **31**, 1683–1690.
- E. W. H. Jager, O. Inganäs and I. Lundström, *Science*, 2000, **288**, 2335–2338.
- J. Kim, J. A. Hanna, R. C. Hayward and C. D. Santangelo, *Soft Matter*, 2012, **8**, 2375–2381.
- Z. B. Hu, Y. Y. Chen, C. J. Wang, Y. D. Zheng and Y. Li, *Nature*, 1998, **393**, 149–152.
- H. Inomata, S. Goto, K. Otake and S. Saito, *Langmuir*, 1992, **8**, 687–690.
- Y. K. Jhon, R. R. Bhat, C. Jeong, O. J. Rojas, I. Szleifer and J. Genzer, *Macromol. Rapid Commun.*, 2006, **27**, 697–701.
- D. J. Beebe, J. S. Moore, J. M. Bauer, Q. Yu, R. H. Liu, C. Devadoss and B. H. Jo, *Nature*, 2000, **404**, 588–590.
- M. Otake, Y. Kagami, M. Inaba and H. Inoue, *Robot. Autonom. Syst.*, 2002, **40**, 185–191.
- F. Peng, G. Z. Li, X. X. Liu, S. Z. Wu and Z. Tong, *J. Am. Chem. Soc.*, 2008, **130**, 16166–16167.
- A. B. Lugao and S. M. Malmonge, *Nucl. Instrum. Methods Phys. Res., Sect. B*, 2001, **185**, 37–42.
- Z. C. Zhu, E. Senses, P. Akcora and S. A. Sukhishvili, *ACS Nano*, 2012, **6**, 3152–3162.
- Y. Li, Z. B. Hu and Y. Y. Chen, *J. Appl. Polym. Sci.*, 1997, **63**, 1173–1178.
- J. Kim, J. A. Hanna, M. Byun, C. D. Santangelo and R. C. Hayward, *Science*, 2012, **335**, 1201–1205.
- P. Techawanitchai, M. Ebara, N. Idota, T. A. Asoh, A. Kikuchi and T. Aoyagi, *Soft Matter*, 2012, **8**, 2844–2851.
- T. S. Shim, S. H. Kim, C. J. Heo, H. C. Jeon and S. M. Yang, *Angew. Chem., Int. Ed.*, 2012, **51**, 1420–1423.
- E. Palleau, D. Morales, M. D. Dickey and O. D. Velev, *Nat. Commun.*, 2013, **4**, 2257.
- A. Phadke, C. Zhang, B. Arman, C. C. Hsu, R. A. Mashelkar, A. K. Lele, M. J. Tauber, G. Arya and S. Varghese, *Proc. Natl. Acad. Sci. U. S. A.*, 2012, **109**, 4383–4388.
- M. M. Zhang, D. H. Xu, X. Z. Yan, J. Z. Chen, S. Y. Dong, B. Zheng and F. H. Huang, *Angew. Chem., Int. Ed.*, 2012, **51**, 7011–7015.
- J. K. Oh, R. Drumright, D. J. Siegwart and K. Matyjaszewski, *Prog. Polym. Sci.*, 2008, **33**, 448–477.
- K. G. Lee, J. Hong, K. W. Wang, N. S. Heo, D. H. Kim, S. Y. Lee, S. J. Lee and T. J. Park, *ACS Nano*, 2012, **6**, 6998–7008.
- G. H. Kwon, Y. Y. Choi, J. Y. Park, D. H. Woo, K. B. Lee, J. H. Kim and S. H. Lee, *Lab Chip*, 2010, **10**, 1604–1610.
- M. C. Cushing and K. S. Anseth, *Science*, 2007, **316**, 1133–1134.
- Z. B. Hu, X. M. Zhang and Y. Li, *Science*, 1995, **269**, 525–527.
- J. Ryu, M. D'Amato, X. D. Cui, K. N. Long, H. J. Qi and M. L. Dunn, *Appl. Phys. Lett.*, 2012, **100**, 161908.
- N. Bassik, G. M. Stern, M. Jamal and D. H. Gracias, *Adv. Mater.*, 2008, **20**, 4760–4764.
- Y. Liu, J. K. Boyles, J. Genzer and M. D. Dickey, *Soft Matter*, 2012, **8**, 1764–1769.
- E. Smela, O. Inganäs and I. Lundström, *Science*, 1995, **268**, 1735–1738.
- X. B. Zhang, C. L. Pint, M. H. Lee, B. E. Schubert, A. Jamshidi, K. Takei, H. Ko, A. Gillies, R. Bardhan, J. J. Urban, M. Wu, R. Fearing and A. Javey, *Nano Lett.*, 2011, **11**, 3239–3244.
- Z. L. Wu, M. Moshe, J. Greener, H. Therien-Aubin, Z. Nie, E. Sharon and E. Kumacheva, *Nat. Commun.*, 2013, **4**, 1586.
- H. Therien-Aubin, Z. L. Wu, Z. Nie and E. Kumacheva, *J. Am. Chem. Soc.*, 2013, **135**, 4834–4839.
- R. Kempaiah and Z. Nie, *J. Mater. Chem. B*, 2014, **2**, 2357–2368.

- 36 W. Hong, Z. Liu and Z. Suo, *Int. J. Solids Struct.*, 2009, **46**, 3282–3289.
- 37 Y. N. Xia and G. M. Whitesides, *Angew. Chem., Int. Ed.*, 1998, **37**, 551–575.
- 38 K. Haraguchi and T. Takehisa, *Adv. Mater.*, 2002, **14**, 1120–1124.
- 39 H. Endo, S. Miyazaki, K. Haraguchi and M. Shibayama, *Macromolecules*, 2008, **41**, 5406–5411.
- 40 K. Haraguchi, H.-J. Li, K. Matsuda, T. Takehisa and E. Elliott, *Macromolecules*, 2005, **38**, 3482–3490.
- 41 S. Miyazaki, H. Endo, T. Karino, K. Haraguchi and M. Shibayama, *Macromolecules*, 2007, **40**, 4287–4295.
- 42 M. Shibayama, T. Karino, S. Miyazaki, S. Okabe, T. Takehisa and K. Haraguchi, *Macromolecules*, 2005, **38**, 10772–10781.
- 43 M. Shibayama, J. Suda, T. Karino, S. Okabe, T. Takehisa and K. Haraguchi, *Macromolecules*, 2004, **37**, 9606–9612.
- 44 S. J. Banik, N. J. Fernandes, P. C. Thomas and S. R. Raghavan, *Macromolecules*, 2012, **45**, 5712–5717.
- 45 P. C. Thomas, B. H. Cipriano and S. R. Raghavan, *Soft Matter*, 2011, **7**, 8192–8197.

## Supporting Information

### **Simulation-assisted Design of Programmable Shape Transformation of Alternating Physical and Chemical Hydrogel Sheets\*\***

*Zengjiang Wei, Zheng Jia, Jasmin Chasmina Athas, Chaoyang Wang, Srinivasa R. Raghavan, Teng Li\*, and Zhihong Nie\**

Z. Wei, J. Athas, Prof. Dr. Z. Nie, Department of Chemistry and Biochemistry, University of Maryland, College Park, MD 20742, USA. Email: [znie@umd.edu](mailto:znie@umd.edu)

Z. Wei, Prof. Dr. C Wang, Research Institute of Materials Science, South China University of Technology, Guangzhou 510640, China.

Z Jia, Prof. Dr. T Li, Department of Mechanical Engineering, university of Maryland, College Park, MD 20742, USA. Email: [LiT@umd.edu](mailto:LiT@umd.edu)

J. Athas, Prof. Dr. S. Raghavan, Department of Chemical and Biomolecular Engineering, University of Maryland, College Park, MD 20742, USA.

## 1. Materials

N-isopropyl acrylamide (NIPAm), N,N'-methylene-bis-acrylamide (MBAA) were purchased from Sigma-Aldrich. 2-Hydroxy-4'-(2-hydroxyethoxy)-2-methylpropiophenone (Irgacure 2959) was purchased from BASF (German). The inorganic clay (a kind of Synthetic Hectorite) Laponite XLG was obtained from Southern Clay Products. NIPAm monomer was purified for twice in hexane using a recrystallization method. Water used in all experiments was purified by deionization and filtration with a Millipore (MA, USA) purification apparatus to a resistivity higher than 18.0 M $\Omega$  cm.

## 2. Fabrication of alternating BG/LG hybrid hydrogel sheets

The alternating BG/LG hybrid hydrogel sheet was fabricated by photopatterning method. The detailed procedures were illustrated in Figure S1. Briefly, an opened rubber O-ring with 800 $\mu$ m thickness was first sandwiched between two glass slides to form a small chamber. The BG precursor was slowly injected into the chamber, and secured by clamps. A photomask with designed patterns was placed on top of the glass slide. The photomask was designed by FreeHand software and printed onto a polymer transparency by a desktop printer (HP laser Jet P3015). The chamber filled with hydrogel precursor was then exposed to ultraviolet (UV) light (Honle UV Technology, UVASPOT 400/T-BL) through the photomask, and selectively to photo-polymerize the hydrogel precursor within exposed area. The chamber was opened and the glass slide was rinsed with water to remove unpolymerized monomers to obtain parallel BG strips on the glass side. The LG precursor was then dropped onto the glass slide to cover the BG strips. The second exposure of the chamber under UV light polymerized LG precursor to produce the BG/LG hybrid hydrogel sheet (See Figure S2a).

*For the first polymerization:* The BG film was synthesized by photo-initiated polymerization of a solution of NIPAm (3g), MBAA (0.2g) and Irgacure 2959 (0.085g) in a deionized water (17g) solution. Firstly, nitrogen gas was bubbled through the mixture for 30 minutes to remove any dissolved oxygen prior to use. After that, the mixture was injected into a reaction chamber, as described above. This reaction chamber was exposed through a mask for 60 s under ultraviolet light irradiation. In the process of photo-polymerization, ice bed was used to cool down the reaction system. Finally, the BG stripe was washed with the deionized water to remove the unreacted precursor to obtain BG stripes on a glass slide.

*For the second polymerization:* The LG film was prepared by polymerizing a solution of NIPAm monomer (3g), Laponite 0.7g, and Irgacure 2959 (0.085g) in (17g) deionized water. After

the solution was bubbled with nitrogen gas for 30 minutes, the precursor of the LG was poured onto the glass slide covered with BG strips. The chamber was clamped and exposed for 60 sec under ultraviolet light irradiation. After the polymerization, the alternating BG/LG hybrid hydrogel sheet was obtained (see Figure S2a). The as-synthesized hydrogel sheet is not fully hydrated on the glass slide and remains flat on the glass slide, possibly due to the physical interactions between the gel and substrate. Upon the immersion of the hydrogel sheet in water, the sheet undergoes shape transformation to form a tubular structure at 25 °C. The detailed recipe of BG and LG was listed in Table S1.

**Table S1: Recipe of BG and LG**

Components	Concentration (wt%)	
	BIS-crosslinked gels (BG)	laponite-crosslinked gels (LG)
NIPAm	13	13
MBAA	1	-
Laponite	-	3
Initiator	0.5	0.5

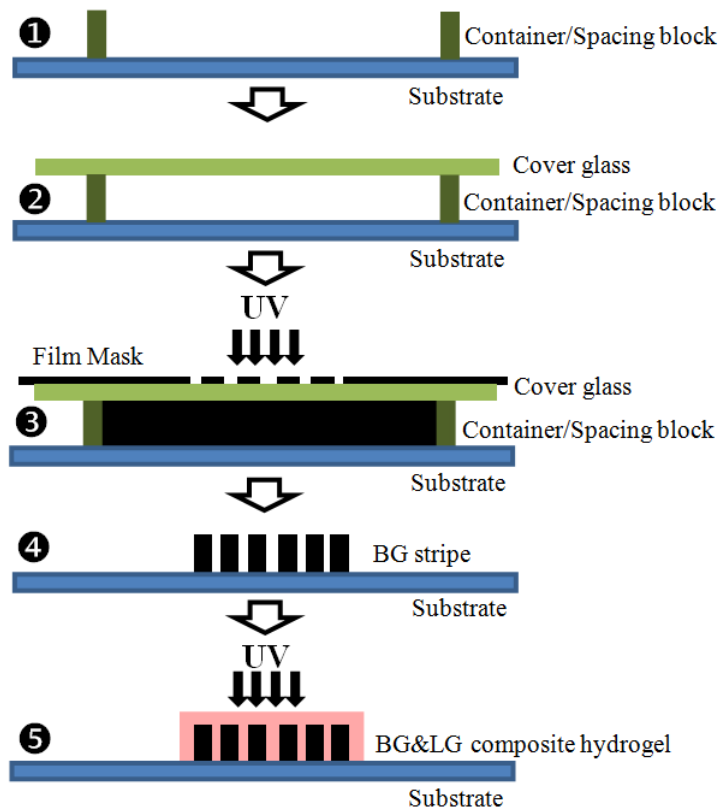


**Figure S1.** Schematic illustration of the fabrication of the BG/LG hybrid hydrogel sheet using multiple-step photopatterning method.

### 3. Formation of the tubular and helical structures through shape transformation of 2D hydrogel sheets

The alternating BG/LG hybrid hydrogel sheet was cut into rectangular samples along the long axis of the strips or along a 45° direction with respect to the long axis of the slender strips. The BG/LG sheet with different cutting angles was removed from glass slide and immersed into deionized water at room temperature. Depending on the cutting angle, the gel sheet transformed into either tubular structures or helical structures (Figure S2).

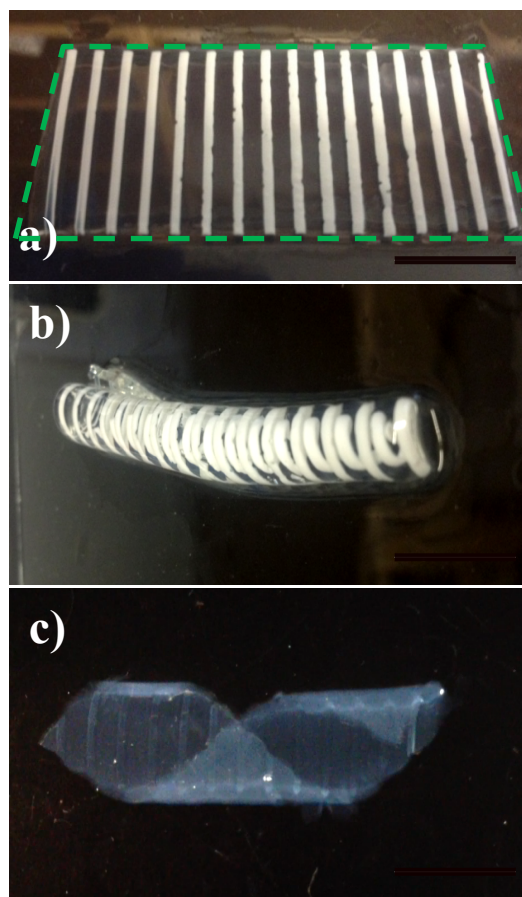


**Figure S2.** (a) A BG/LG hybrid hydrogel sheet on a glass slide. (b,c) After the immersion of the gel sheet in DI water at room temperature, the hydrogel sheet transformed into tubular structure (b) or helical structure (c), depending on the cutting angle. Scale bars are 1cm.

#### 4. Mechanical properties determined by rheology

Rheological experiments were performed on a RDA-III strain controlled rheometer (TA Instruments). All rheological experiments were done at 25 °C using parallel plate geometry (25 mm diameter). A solvent trap was used to minimize drying of the samples. Dynamic frequency sweeps were conducted within the linear viscoelastic regime of the sample, which was determined separately from strain sweep experiments.

#### 5. Simulation of the shape transformation of hybrid hydrogel sheets

To simulate the deformation of hybrid hydrogel sheets, we employ the method developed by Hong *et al.* to implement a finite element method for gels [S1]. The Helmholtz free energy function according to Flory and Rehner [S2] is separable into contributions from stretching the polymeric network and mixing the polymer and the solvent:

$$W(F, C) = W_{stretch}(F) + W_{mix}(C), \quad (1)$$

where  $F$  is the deformation gradient tensor and  $C$  is the concentration of the solvent in the gel. In the original Flory-Rehner model,  $W_{stretch}$  represents the free energy due to stretching of the polymeric network and is taken to be

$$W_{stretch} = \frac{1}{2}NkT(F_{iK}F_{iK} - 3 - 2\log(J)), \quad (2)$$

where  $N$  is the number of polymer chains per unit volume,  $kT$  is the temperature in the unit of energy, and  $J = \det(F)$ . The free energy associated with mixing the polymer and the solvent is represented by  $W_{mix}(C)$  and is given by

$$W_{mix} = \frac{kT}{v} \left[ vC \log\left(\frac{vC}{1+vC}\right) - \frac{\chi}{1+vC} \right] \quad (3)$$

where  $v$  represents the volume of one solvent molecule and  $\chi$  is a dimensionless measure of the enthalpy of mixing, which describes the interaction between the solvent and the polymer. The molecular incompressibility requires that  $\det(F) = 1 + vC$ , which applies a constraint between deformation and solvent concentration.

To implement this hydrogel model in finite element method, another free-energy  $\hat{W}(F, \mu)$  can be introduced by Legendre transformation:

$$\hat{W}(F, \mu) = W(F, C) - \mu C \quad (4)$$

Here,  $\mu$  is the chemical potential prescribed by the environment. By introducing  $\hat{W}(F, \mu)$ , the equilibrium state of the gel can be expressed as

$$\int \delta \hat{W} dV = \int B_i \delta x_i dV + \int T_i \delta x_i dA \quad (5)$$

This equilibrium condition takes the same form as the weak-form equilibrium equation of hyperelastic solids in ABAQUS. Therefore, once the explicit form of  $\hat{W}(F, \mu)$  is given, we can implement a finite element method in ABAQUS through a UHYPER user-subroutine. More details about the finite element method implementation and the UHYPER user-subroutine can be found in Ref. S1.

Combining Eqs. (1-4) and the molecular incompressibility gives the  $\hat{W}$  as

$$\frac{\hat{W}v}{kT} = \frac{1}{2}Nv(F_{iK}F_{iK} - 3 - 2\log(J)) - \left[ (J-1)\log\left(\frac{J}{J-1}\right) + \frac{\chi}{J} \right] - \frac{\mu}{kT}(J-1) \quad (6)$$

As noted in the main text, Eq. (6) indicates that the system has two independent material properties: the normalized nominal density of polymer chains  $Nv$  and the enthalpy of mixing  $\chi$ . The values of the material properties used in our simulations can be found in Table S2. When the gel with initial chemical potential  $\mu_0$  is submerged in a solvent with environmental chemical potential  $\mu$ , the gel absorbs (when  $\mu_0 < \mu$ ) or loses (when  $\mu_0 > \mu$ ) water until its chemical potential is equal to chemical potential of the external solvent  $\mu$ . In our simulations, we tune the initial chemical potential  $\frac{\mu_0}{kT}$  and the solvent chemical potential  $\frac{\mu}{kT}$  to simulate the volume change of the hybrid hydrogel sheets observed in the experiments.

### References:

- S1. Hong W., Liu Z. S., Suo Z. G. Inhomogeneous swelling of a gel in equilibrium with a solvent and mechanical load. *Int. J. Solids Struct.*, **46** (2009) 3282-3289.  
 S2. Flory, P.J., Rehner, J., Statistical mechanics of cross-linked polymer networks II swelling. *J. Chem. Phys.* **11** (1943), 521–526.

**Table S2:** Parameters used in simulations

Hybrid hydrogel sheet		#1	#2	#3
<b>BG</b>	Nv	0.0015	0.0007	0.0001
	X	0.6		
<b>LG</b>	Nv	0.001		
	X	0.01		

**Table S3:** List of four modes of shape transformation of hybrid hydrogel sheets

Rolling direction Rolling axis	BG wrapped inside	BG exposed outside
Normal to BG strips	Model 1	Model 2
Parallel to BG strips	Model 3	Model 4

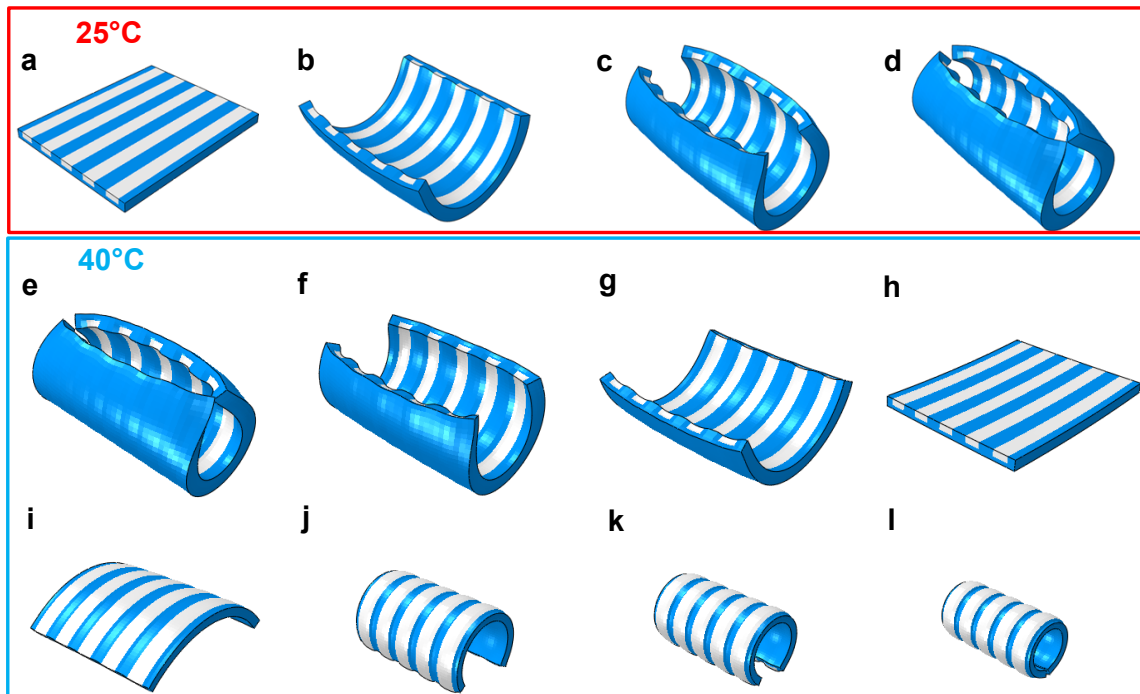


**Figure S3.** Simulated shape-transformation process of an as-made planar hybrid hydrogel sheet into a Mode 1 tubular structure in 25°C water (a-d). When immersed in 40°C water, such a Mode 1 tubular structure first unfolds and flattens (e-h), and further rolls in the opposite direction toward another tubular structure (Mode 2) (i-l).

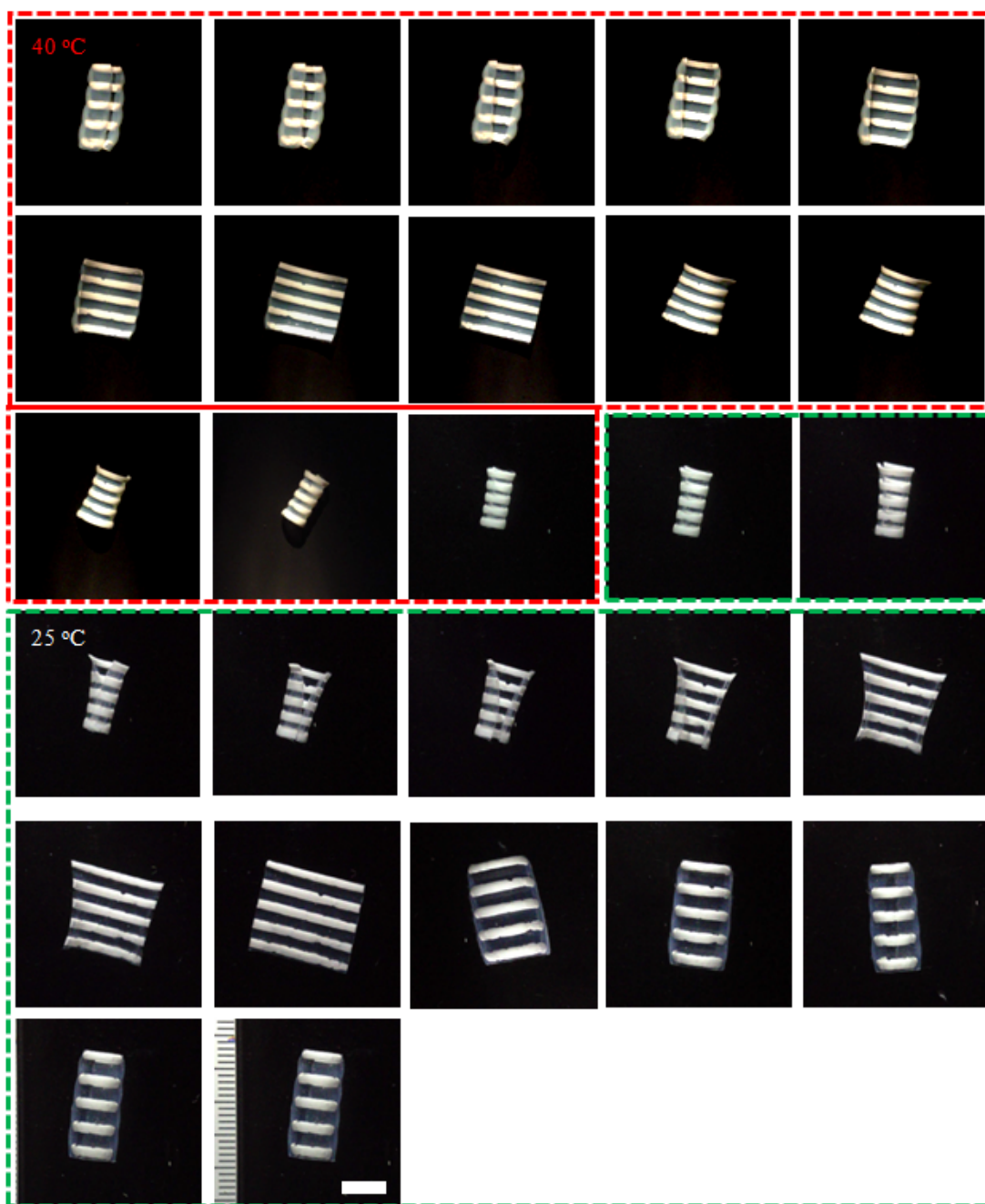


**Figure S4.** The time-dependent shape transformation of hybrid hydrogel sheet in response to temperature change. When immersed in water at 40 °C, the tubular structure in Mode 1 opens up and flattens, then further rolls into a tubular structure with the BG strips exposed outside (denoted as Mode 2) (in red dashed frame). Upon the further immersion of the structure in Mode 2 in water at 25 °C, the tubular structure transits to Mode 1 (in green dashed frame). The transition between Mode 1 and Mode 2 are reversible and repeatable. Scale bar is 0.5 cm.

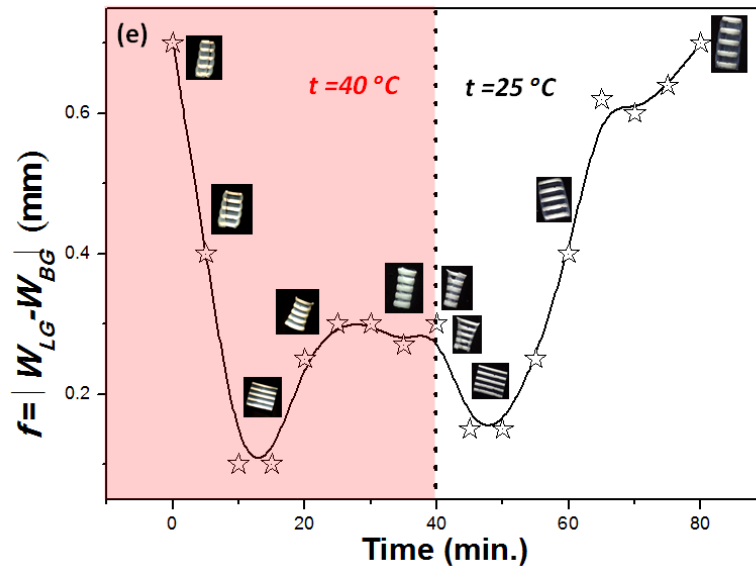
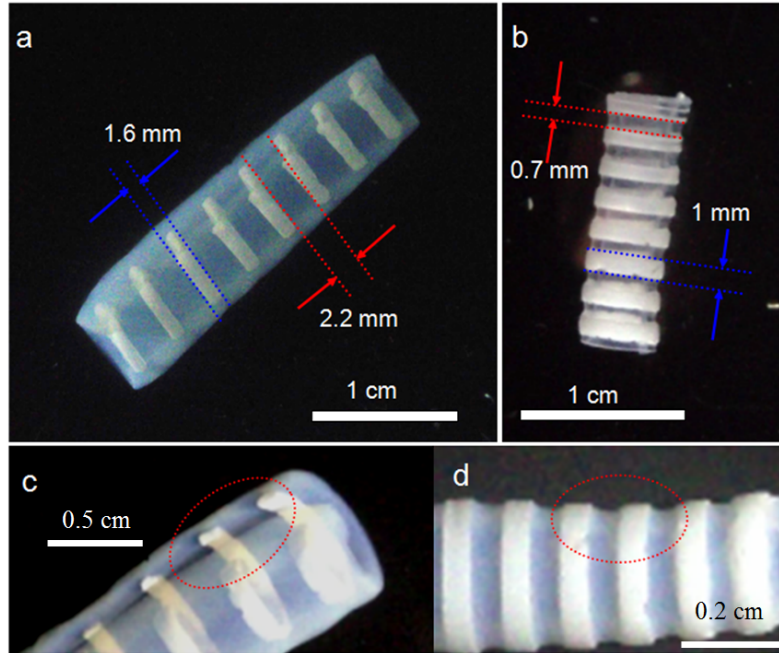


**Figure S5.** (a, b) Photos showing the dimension of the transformed structures of hybrid hydrogel sheets in 25°C water (Mode 1, tubular structure with the BG strips hidden in the interior of the tube) (a) and in 40°C water (Mode 2, tubular structure with the BG strips exposed outside) (b). (c,d) A close inspection of the hydrogel sheet in Mode 1 (c) and in Mode 2 (d). It is clear that the BG strips are wrapped inside in Mode 1 (c), while the outer surface of tubular structure in Mode 2 show undulation morphology with BGs at peaks and LGs at troughs (d). (e) The difference between LG strip width  $W_{LG}$  and BG strip width  $W_{BG}$ , as a function of time after a tubular

hydrogel sheet in Mode 1 first immersed in 40 °C water and then in 25 °C water. Optical images in (e) show the reversible transition from Mode 1 to Mode 2 and back to Mode 1.

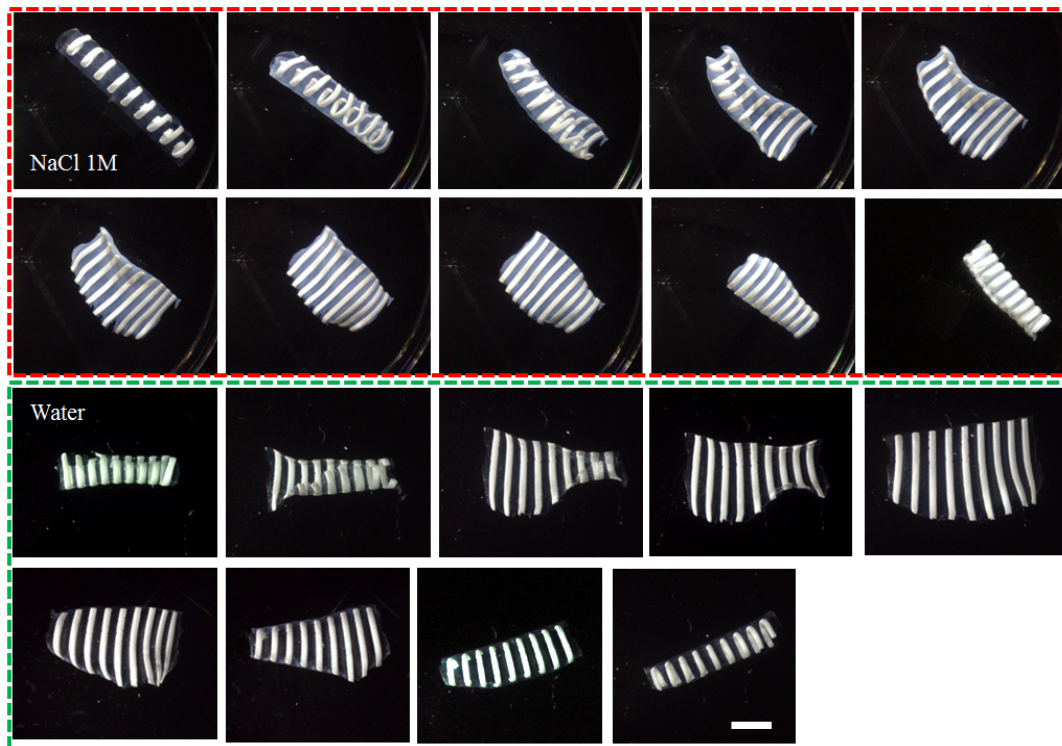


**Figure S6.** The time-dependent shape transformation of hybrid hydrogel sheet in response to the concentration of salt in solution (corresponding to ionic strength). When immersed in 1M NaCl solution, the tubular structure in Mode 1 opens up and flattens, then further rolls into a tubular structure with the BG strips exposed outside (denoted as Mode 2) (in red dashed frame). Upon the further immersion of the structure in Mode 2 in pure water (without NaCl), the tubular structure transits to Mode 1 (in green dashed frame). The transition between Mode 1 and Mode 2 are reversible and repeatable. The temperature is 25 °C. Scale bar is 1cm.

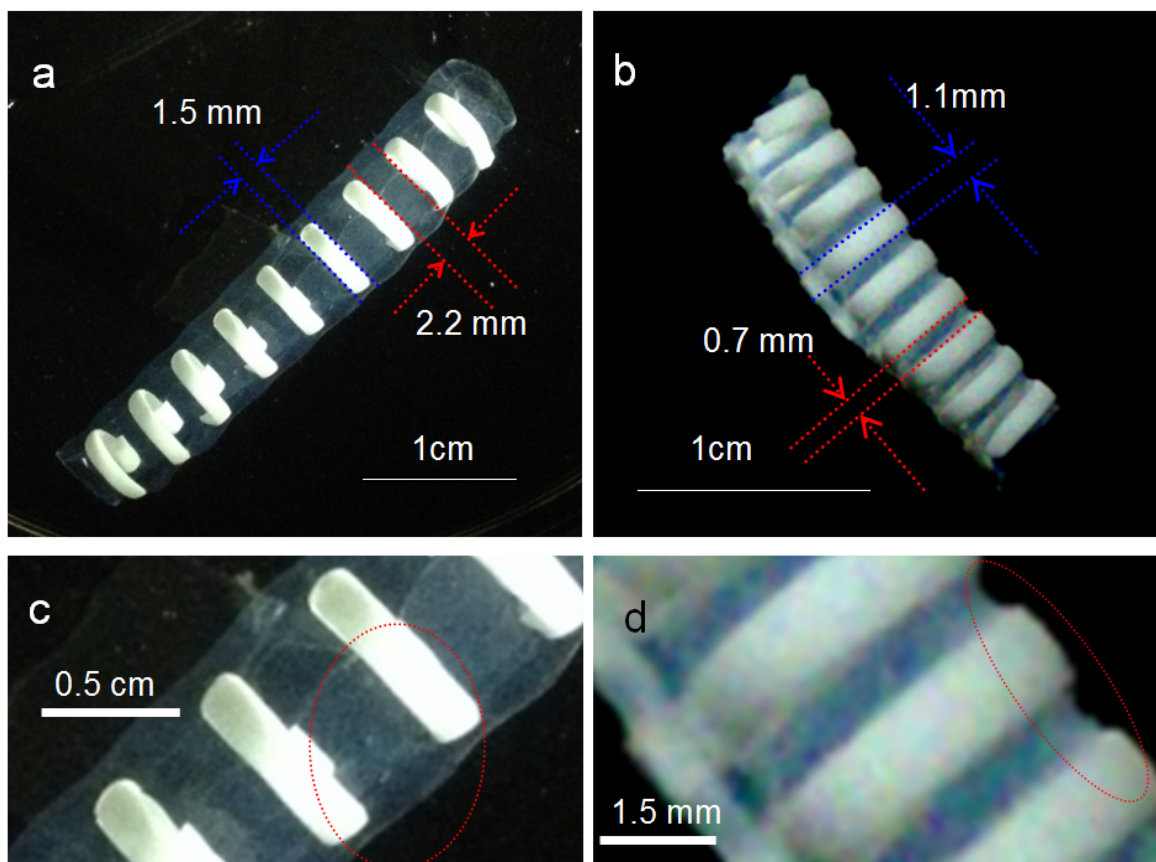


**Figure S7.** (a, b) Photos showing the dimension of the transformed structures of hybrid hydrogel sheets in pure water (Mode 1) (a) and 1M NaCl solution (Mode 2) (b). (c,d) A close inspection of the hydrogel sheet in Mode 1 (c) and in Mode 2 (d). The temperature is 25 °C.

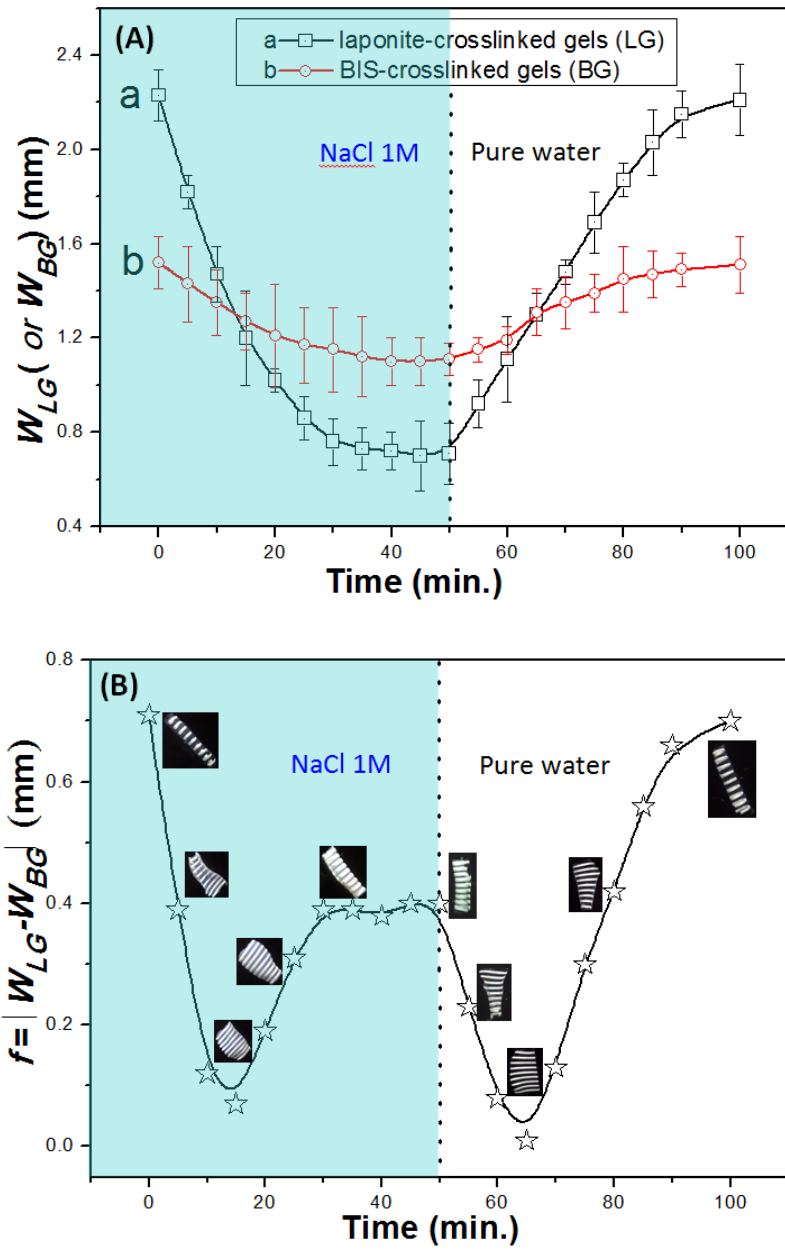


**Figure S8.** (A) Variation in the BG strip width  $W_{BG}$  (red) and LG strip width  $W_{LG}$  (dark), and (b) the difference between  $W_{LG}$  and  $W_{BG}$ , as a function of time after a tubular hydrogel sheet in Mode 1 was first immersed in 1M NaCl solution and then in pure water. Optical images in (B) show the reversible transition from Mode 1 to Mode 2 and back to Mode 1.

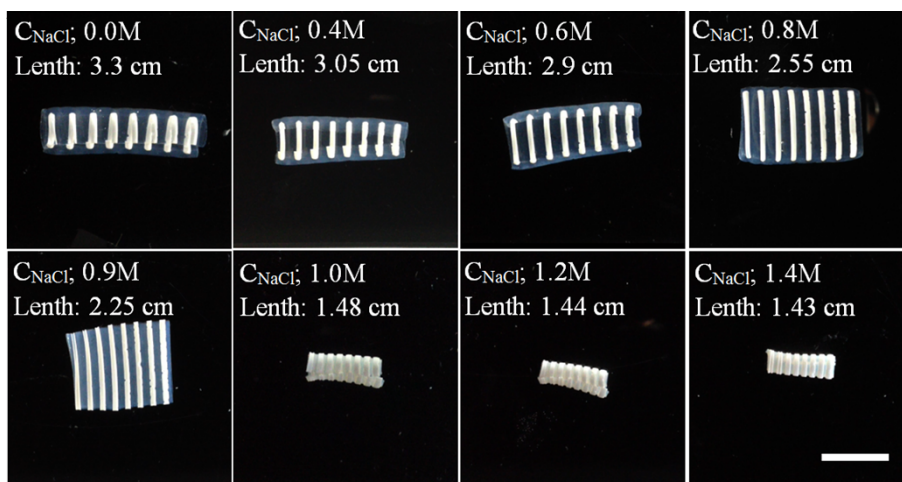


**Figure S9.** The dimension of the hybrid hydrogel sheets in a NaCl solution with different concentration of salt. Scale bar 1.5cm.

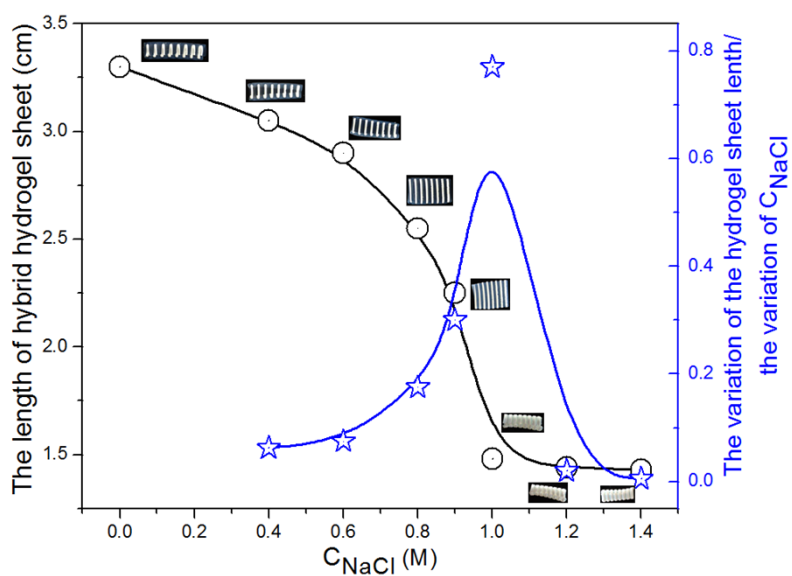


**Figure S10.** The length of the hybrid hydrogel sheet (left y-axis) and the variation in the length of the hydrogel sheet (right y-axis) as a function of the concentration of NaCl in an aqueous solution. Inset images show the shape-transformed 3D structures.

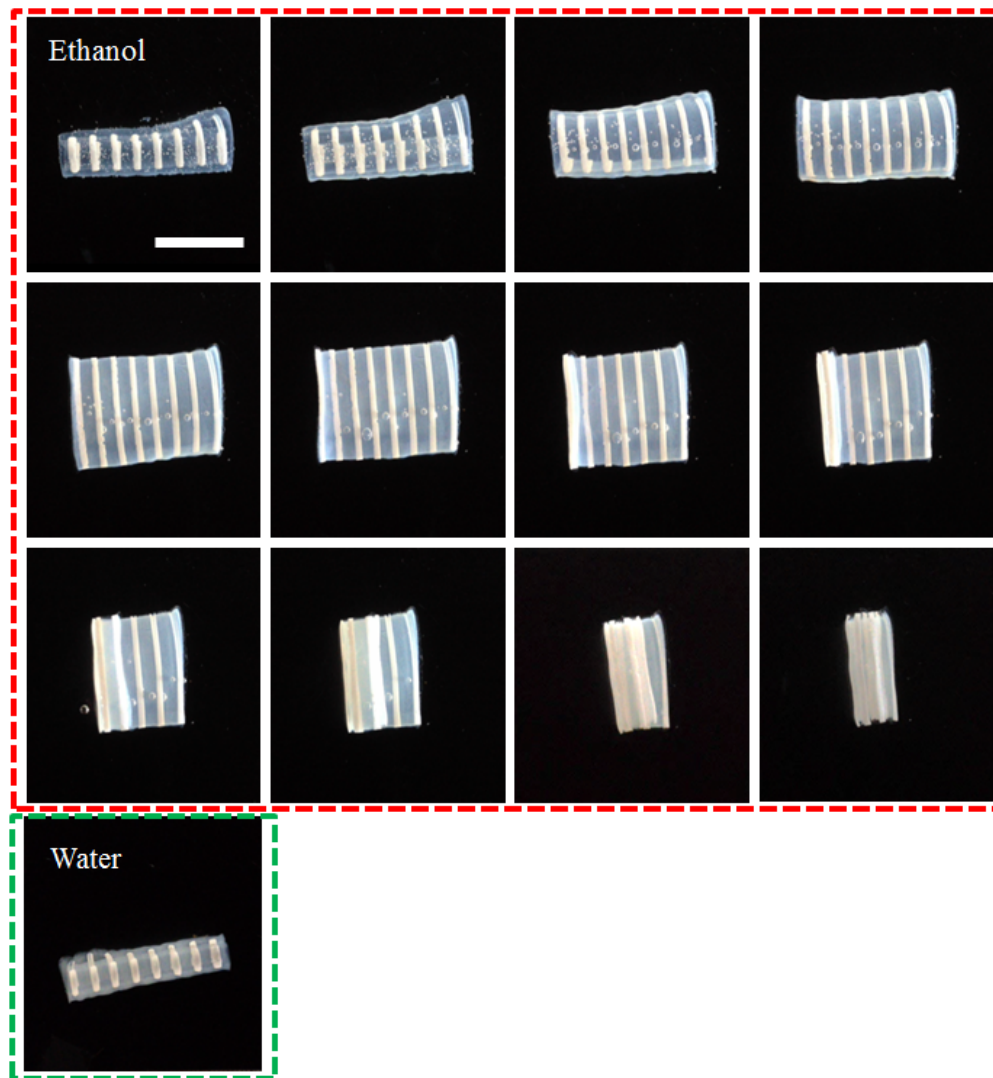


**Figure S11.** The time-dependent shape transformation of hybrid hydrogel sheet in response to ethanol solvent (in red dashed frame) at 25 °C. When immersed in ethanol, the tubular structure in Mode 1 opens up and flattens, then further roll about an axis parallel to the BG strips into another tubular structure with BG strips hidden inside (denoted as Mode 3). The hydrogel sheet recovers to its original Mode 1 in purewater at 25 °C (green dashed frame). The transformation between Mode 1 and 3 is fully reversible. Scale bar is 1.5cm.